Bone Reports 21 (2024) 101773

Contents lists available at ScienceDirect

Bone Reports

journal homepage: www.elsevier.com/locate/bonr

Bone collagen tensile properties of the aging human proximal femur

Stefan Bracher [a,*], Benjamin Voumard [a], Mathieu Simon [a], Tatiana Kochetkova [a], Michael Pretterklieber [b,c], Philippe Zysset [a]

[a] ARTORG Center for Biomedical Engineering Research, University of Bern, Switzerland
[b] Division of Macroscopic and Clinical Anatomy, Gottfried Schatz Research Center, Medical University of Graz, Austria
[c] Division of Anatomy, Center for Anatomy and Cell Biology, Medical University of Vienna, Austria

ARTICLE INFO

Keywords:
Cortical bone
Collagen type I
Raman spectroscopy
Tensile strength
micro-CT
Gravimetric analysis

ABSTRACT

Despite the dominant role of bone mass in osteoporotic fractures, aging bone tissue properties must be thoroughly understood to improve osteoporosis management. In this context, collagen content and integrity are considered important factors, although limited research has been conducted on the tensile behavior of demineralized compact bone in relation to its porosity and elastic properties in the native mineralized state. Therefore, this study aims (i) at examining the age-dependency of mineralized bone and collagen micromechanical properties; (ii) to test whether, and if so to which extent, collagen properties contribute to mineralized bone mechanical properties.

Two cylindrical cortical bone samples from fresh frozen human anatomic donor material were extracted from 80 proximal diaphyseal sections from a cohort of 24 female and 19 male donors (57 to 96 years at death). One sample per section was tested in uniaxial tension under hydrated conditions. First, the native sample was tested elastically (0.25 % strain), and after demineralization, up to failure. Morphology and composition of the second specimen was assessed using micro-computed tomography, Raman spectroscopy, and gravimetric methods. Simple and multiple linear regression were employed to relate morphological, compositional, and mechanical variables with age and sex.

Macro-tensile properties revealed that only elastic modulus of native samples was age dependent whereas apparent elastic modulus was sex dependent ($p < 0.01$). Compositional and morphological analysis detected a weak but significant age and sex dependency of relative mineral weight ($r = -0.24$, $p < 0.05$) and collagen disorder ratio ($I_{\sim1670}/I_{\sim1640}$, $r = 0.25$, $p < 0.05$) and a strong sex dependency of bone volume fraction while generally showing consistent results in mineral content assessment. Young's modulus of demineralized bone was significantly related to tissue mineral density and Young's modulus of native bone.

The results indicate that mechanical properties of the organic phase, that include collagen and non-collagenous proteins, are independent of donor age. The observed reduction in relative mineral weight and corresponding overall stiffer response of the collagen network may be caused by a reduced number of mineral-collagen connections and a lack of extrafibrillar and intrafibrillar mineralization that induces a loss of waviness and a collagen fiber pre-stretch.

1. Introduction

Osteoporosis is a systemic, metabolic skeletal bone disease identified by reduced bone mass and microstructural deterioration, resulting in increased bone fragility and sensitivity to fracture ("Consensus development conference," 1993). In 2019 in Switzerland, one woman out of two and one man out of five sustained an osteoporotic fracture after the age of 50 years (Ferrari et al., 2020). Such fractures cause pain, reduce mobility, and increase mortality while substantially increasing healthcare costs, presenting a significant challenge in an aging society (Kling et al., 2014).

Despite bone mass's dominant role in osteoporotic fracture (Compston et al., 2019), bone strength determinants must be thoroughly investigated on both micro and macro scale to improve osteoporosis

* Corresponding author at: University of Bern, ARTORG Center for Biomedical Engineering Research, Department of Musculoskeletal Biomechanics, Sitem Insel, Freiburgstrasse 3, 3010 Bern, Switzerland.
E-mail address: stefan.bracher@unibe.ch (S. Bracher).

https://doi.org/10.1016/j.bonr.2024.101773
Received 20 November 2023; Received in revised form 11 April 2024; Accepted 10 May 2024
Available online 13 May 2024

management, specifically the function of tissue aging. In this context, collagen integrity, content, and structure are considered major parameters, although little research has been conducted on demineralized human compact bone tissue to date, which relates its characteristics to porosity and elastic properties in the native mineralized state (Bailey et al., 1999; Boskey et al., 1999; Garnero, 2012; Viguet-Carrin et al., 2006; Wang et al., 2001).

Zioupos (Zioupos, 2001) investigated each bone tissue phase's kind and relative contribution to the biomechanical behavior of ten human femoral cortical bone tissue specimens. Among several compositional and mechanical variables, the shrinkage temperature and the maximum normalized rate of load contraction were assessed by means of isometric shrinkage experiments. It was found that both exhibit significant negative correlations with age ($r < -0.63$, $p < 0.05$), indicating that older bone possesses more regions of remodeled tissue, which is believed to be richer in heat labile aldimine bonds. In addition, several positive significant correlations were obtained between those two factors and several toughness properties, such as J-integral, fracture toughness, and work to fracture. In contrast, the toughness properties showed significant negative correlations with age. It was concluded that the increase in bone fractures with age is partially due to a decrease in toughness of bone tissue, which is reduced because of a deterioration of the collagen network. In a more recent study (Bonicelli et al., 2022) assessment of micromechanical, compositional, and physicochemical properties in cortical rib bone revealed that skeletal maturity is reached at around 35 years of age, leading to a change in the age trends of various parameters.

Similarly, Wang et al. (Wang et al., 2002) hypothesized that the mechanical integrity of the collagen network in bone deteriorates with age and that these changes correlate with a decreased toughness of aged bone. Therefore, 80 human anatomic femoral specimens from donors ranging from 19 to 89 years of age at death were tested in both mineralized and demineralized states, investigating various morphological and mechanical characteristics. Besides various correlations found between morphological and mechanical variables in the mineralized samples, experimental results indicated that the mechanical integrity of the collagen network deteriorates with increasing age and correlates significantly with a decreasing work to fracture of aged bone. Burr et al. (Burr, 2002) pointed out that one component of the increased tissue fragility in the elderly is the older mean tissue age due to a declining bone turnover rate. In contrast, molecular changes in organic or inorganic portions of the matrix may further serve as a suitable explanation. However, Wang (Wang et al., 2002) also investigated collagen cross-links and collagen denaturation as a function of age and found that the number of enzymatic cross-links, such as hydroxylysylpyridinoline (HP) and lysylpyridinoline (LP), did not significantly correlate with age. Further, they observed that the amount of non-enzymatic cross-links, i.e., pentosidine (PE), significantly increased with age. Thus, it was proposed that advanced glycation end products (AGEs) assessed using pentosidine concentration are one of the major causes of age-related changes in the collagen network and bone quality, as those accumulate with aging. Similar findings have been made in other studies (Nyman et al., 2007; Odetti et al., 2005; Oxlund et al., 1995; Saito et al., 1997; Saito and Marumo, 2010).

Nevertheless, a recent review by Willet et al. (Willett et al., 2022) concluded that while there is plenty of in vitro evidence that AGEs decrease bone toughness, in vivo evidence of AGE accumulation is sparse. Interestingly, the role of AGE adducts, which are far more abundant than AGE cross-links, in the mechanical behavior of bone has yet to be established. This role is thought of particular importance since an accumulation of those adducts could potentially hinder enzymatic cross-linking and negatively impact stabilizing interactions among collagens, mineral, water, and non-collagenous proteins (NCPs). In contrast, a recent study by Britton et al. (Britton et al., 2023) investigated the effects of in vitro induced AGEs on bovine cortical bone fracture mechanics at fall-related loading rates and found no evidence that AGEs alone affect bone fragility. Instead, AGE accumulation was found to positively alter pre- and post-yield properties such as yield stress ($p = 0.001$), ultimate flexural strength ($p = 0.018$), secant modulus ($p = 0.05$), critical fracture toughness ($p = 0.007$), and contribution of elastic phase to non-linear J-integral ($p = 0.007$).

Characterization of the mineral compartment of bone is frequently done by histology analysis, although this method is restricted to 2D analysis. Thus, micro-computed tomography (μCT) is employed to evaluate bone morphology on ex vivo samples providing high resolution 3D images (Feldkamp et al., 1989; Kuhn et al., 1990). Following the basic principles of clinical CT, a specimen is placed in the path of an x-ray beam generating a projection image on a x-ray-sensitive detector. A 3D volume is reconstructed by stacking of the projections which are consecutively collected after rotating the sample multiple times.

As experimental methods and measurement device reliability have been tremendously improved over the past 20 years, and since no similar studies were conducted in the meantime for a large cohort, the present work aims (i) at partially reproducing the results obtained by Wang, i.e., to examine the age-dependency of mineralized bone and collagen micromechanical properties; (ii) to test whether, and if so to which extent, collagen properties contribute to mineralized bone mechanical properties.

2. Methods

2.1. Sample origin

Eighty, 60 mm long fresh frozen anatomic specimens of human bone sections from the proximal part of the femoral diaphysis of 19 male, 24 female, and of one unspecified donor with a median age at death of 81 (57 to 96) years were used in this study. For some donors, samples of both left and right sides were used. The age of the female donors varied from 71 to 96 years at death, and one of the male donors from 64 to 85 years at death. Lifestyle, medication history, and disease state were unknown. The specimens were provided by the Division of Anatomy of the Medical University of Vienna. Informed consent of the donors has been obtained. The specimens were frozen at −20 °C immediately after dissection.

2.2. Sample preparation

Two samples were extracted from each section's proximal, lateral side (4 mm × 25 mm) by manual drilling (JET Promac 370E, Walter Meier (Tool) AG, Fällanden, Switzerland) (Fig. 1). Thereby, the bone sections were oriented along the long axis of the femur and fully immersed in 0.9 w% NaCl solution. Subsequently, the bone sections were cut perpendicular to the long axis of the cylindrical samples using a diamond band saw (30/741, EXAKT Apparatebau GmbH, Norderstedt, Germany) under constant water irrigation (Fig. 1).

Bone samples were immersed into acetone (Aceton ≥99.5 %, VWR International GmbH, Dietikon, Switzerland) and stirred for 15 min (TL 10, Edmund Bühler GmbH, Bodelshausen, Germany) to remove any soft tissue. Subsequently, superficial liquid on the sample surface was blotted dry, and samples used for mechanical testing were glued into an aluminum cylinder using 2-component epoxy adhesive (Araldite 2014–2, Huntsman International LLC, Everberg, Belgium), and cured at room temperature for two days. Samples that underwent gravimetric analysis were refrozen upon soft tissue removal.

Lateral holes of diameter 6.0 mm were drilled manually on a pillar drilling machine (Fehlmann P10, Fehlmann AG, Seon, Switzerland). The final sample geometry was produced on an engineering lathe (Schaublin 1185, Schaublin Machines SA, Bévilard, Switzerland), exhibiting a gauge section of 2 mm in diameter and 6.5 mm in length. In total, 160 specimens (90 female, 68 male, 2 unknown sex/age) were prepared for mechanical assessment (80 samples) and gravimetric analysis (80 samples), of which 6 specimens broke before reversible mechanical testing and an additional 3 before failure testing.

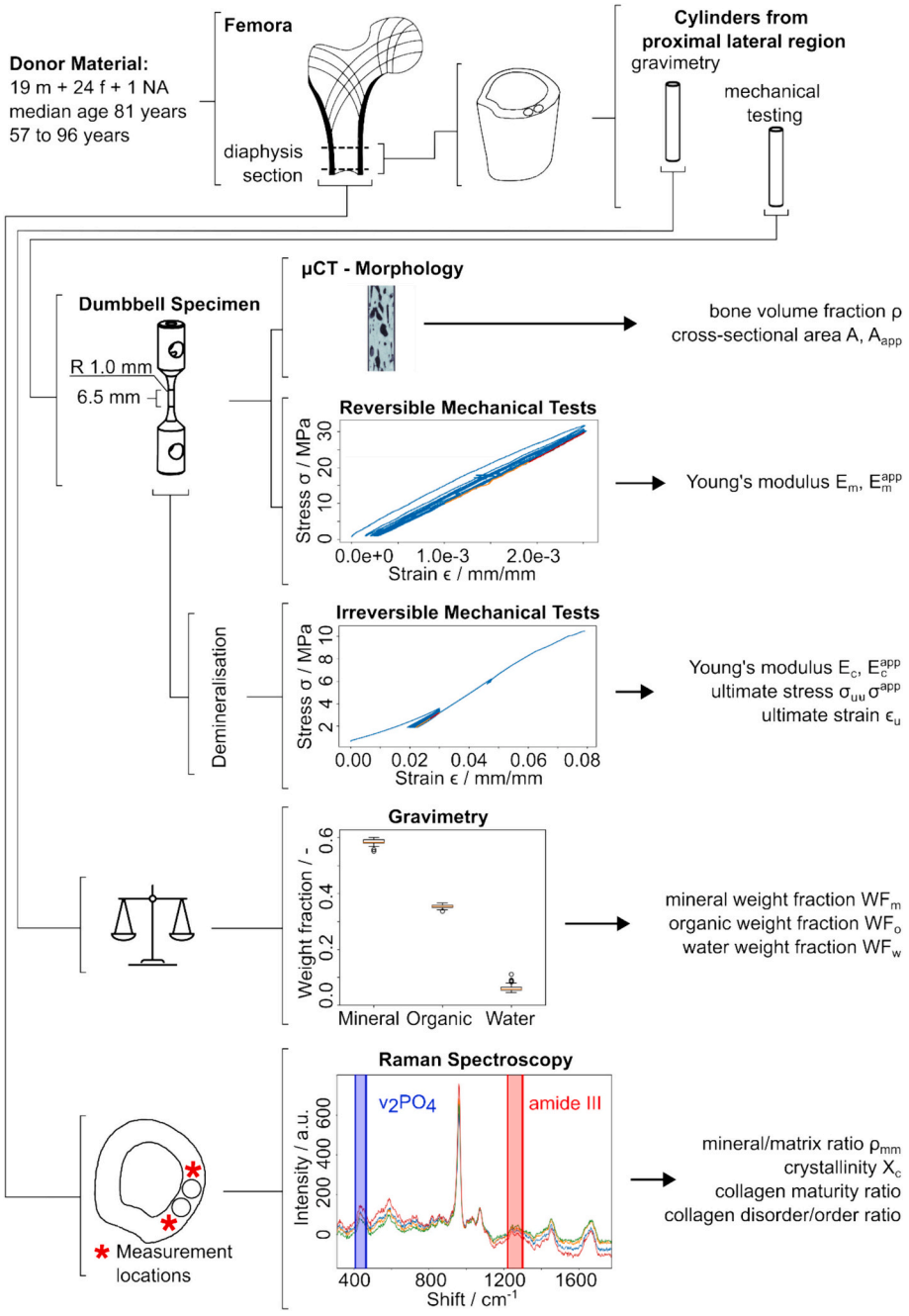

Fig. 1. The study overview illustrates the combination of different experimental techniques used.

2.3. Micro CT imaging

For morphology analysis, a 7 mm long, central section was scanned in a micro computed tomography (µCT) scanner (µCT 100, SCANCO Medical AG, Brüttisellen, Switzerland) at a spatial resolution of 7.4 µm and a field of view (FOV) of 15.2 mm. Samples were submerged in 0.9 w % NaCl solution during scanning and refrozen afterward. X-ray tube voltage, current, and integration time were set to 70 kVp, 200 µA, and 200 ms, respectively, while using an aluminum filter with a thickness of 0.5 mm. Data averaging was set to 1 (one image acquired per projection). Image processing was performed using Python (Version 3.11.4) (Van Rossum and Drake, 2009). Images were cropped manually and then segmented using Otsu's method, leading to binary images (bone and no bone). The total volume was approximated by fitting an ellipse to the sample's outer hull, which was expanded along the longitudinal axis to form a cylinder. Bone volume fraction ρ was defined as bone volume normalized by the volume of the whole cylinder. Tissue mineral density (TMD) was computed as the bone volume's mean bone mineral density (BMD). The mean apparent area A_{app} and mean bone area A were defined as the average cross-sectional area of the cylinder and the average bone area per slice, respectively.

2.4. Tensile testing

For macroscopic mechanical testing, specimens were re-hydrated in 0.9 w% NaCl solution for 12 h at 4 °C and kept in NaCl at room temperature for at least 2 h to reach thermal equilibrium (Mirzaali et al., 2016). Reflective particles (Albedo 100 Permanent Transparent, TrackInvent AB, Helsingborg, Sweden) were applied on a black background layer on ≈1 mm wide regions at the gauge sections ends to

enhance contrast for optical tracking. Subsequently, samples were immediately tested.

Tests were performed in uniaxial tension using a multipurpose servo-hydraulic testing system (MTS 858 Mini Bionix, MTS Systems Corp., Minnesota, United States) equipped with a video extensometer (laserXtens 1-15 HP, ZwickRoell GmbH & Co. KG, Ulm, Germany) with a resolution of ~ 0.04 µm (Fig. 2). Reaction forces were measured employing an s-beam load cell (RL20000A-100 SS, Rice Lake Weighing Systems, Wisconsin, United States) with a load capacity of 450 N. The samples were fixed in a support device by inserting two fixation pins. Quasi-static tests were performed at a strain rate of $\approx 1.8 \bullet 10^{-3}$ s^{-1} (displacement rate of $1.2 \bullet 10^{-2}$ mm s^{-1}). Native samples were pre-conditioned for eight cycles up to 0.25 % strain in tension, using displacement-controlled mode. Stress on the apparent σ_{app} and intrinsic σ level was calculated as F/A_{app} and F/A, respectively. Engineering strain $\epsilon = \Delta l \bullet l^{-1}$ in tension was calculated using the displacement Δl, recorded by the extensometer and the original length l of the gauge section.

Young's Modulus of the native (mineralized) bone samples on the apparent E_m^{app} and intrinsic E_m level was calculated as the slope of the corresponding apparent and intrinsic stress-strain curve's unloading part of the last preconditioning cycle employing a moving linear regression with a 33 % window width (one-third of the length) to identify the steepest section.

All tests were performed at approximately 23 °C and 45 % relative humidity. Data was acquired at a sampling rate of 100 Hz with a test duration between 2.5 and 5.5 min. Time, displacement (videoXtens Version 6.10.0.0, ZwickRoell GmbH & Co. KG, Ulm, Germany), and force (MTS FlexTest Station Manager Version 5.8B 5713, MTS System Corp., Minnesota, United States) were recorded simultaneously.

2.5. Decalcification

Samples were decalcified by immersion in buffered (pH 7.4) 0.5 mol/L ethylene-diamine tetra acetic acid (EDTA disodium salt dihydrate ≥99 %, Thermo Fisher Scientific, Kandel, Germany) solution at approximately 23 °C for 12 days with changes of the solution every two days (Zioupos et al., 1999). The demineralization process was tracked by visually inspecting µCT scout view images and was found to be finished when no more bone could be visually identified, i.e., after ten days; therefore, the duration was extended to 12 days. Scout views were preferred over complete 3D scans to minimize sample X-ray exposure as multiple ex vivo studies on both cortical and trabecular bone demonstrate that ionizing radiation deteriorates mechanical properties i.e., ultimate strain, ultimate strength, fracture toughness, and work-to-failure but also collagen molecular structure independently of cellular activity (Akkus and Rimnac, 2001; Barth et al., 2011, 2010; Burton et al., 2014; Currey et al., 1997; Nguyen et al., 2007). The reduction of those properties of irradiated bone could be assigned to structural changes of collagen on the molecular level (Burstein et al., 1975; Nyman et al., 2005; Zioupos et al., 1999). After demineralization, samples were rinsed with water for 2 min, blotted dry, and refrozen.

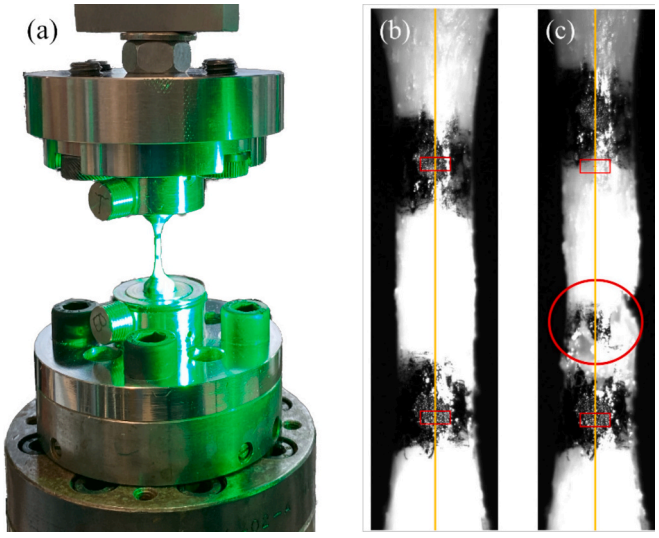

Fig. 2. Uniaxial tensile testing setup (a) and demineralized sample (right) prior to (b) and after (c) failure testing, indicating the tracking area (red rectangles), the axial symmetry (yellow line), and the failure region (red circle). The image was recorded using videoXtens software.

2.6. Failure testing

Similarly, fully demineralized samples were preconditioned for eight cycles between 2 and 3 % strain in tension using displacement-controlled mode and subsequently monotonically loaded to failure using the same strain rate (Fig. 3). Calculation of apparent and intrinsic stress, strain, and Young's modulus on the apparent E_o^{app}, and intrinsic E_o level of the organic matrix followed the same principle as described above. Ultimate stress σ_u, ultimate apparent stress σ_u^{app}, and ultimate strain ϵ_u were calculated as the maximum stress and corresponding strain.

2.7. Gravimetric analysis

Samples were weighed in wet, dry, and ashed conditions (LAG 314i, VWR International, Leuven, Belgium). Samples were considered wet when immersing in dH2O for 48 h and subsequent centrifugation (5415 R, Eppendorf AG, Hamburg, Germany) at 15 relative centrifugal force for 5 min. Previous testing revealed no significant difference in sample weight when increasing immersion time, centrifugation force, or time. Immediately following centrifugation, wet weights in grams were acquired.

Samples were dried and ashed (LVT 3/11, Nabertherm GmbH, Lilienthal/Bremen, Germany) at 40 °C for 48 h (Unal et al., 2014) and 800 °C for 12 h (Wang et al., 2002), respectively. Dry and ashed weights in grams were acquired immediately after removal from the furnace. The weight fractions of mineral (WF_m) and organic phases (WF_o) were calculated by dividing the weight of ash residue and weight of the organic phase by wet weight of bone, respectively (Wang et al., 2002).

2.8. Raman spectroscopy

Raman spectra were recorded using a portable, fiber optic Raman

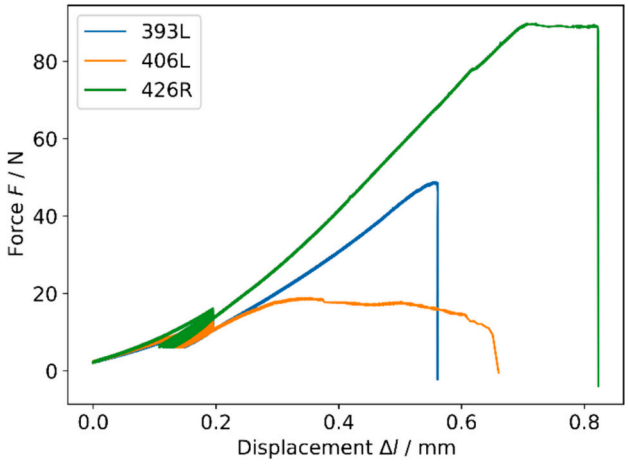

Fig. 3. Force/displacement curves of three arbitrary samples showing brittle (blue), ductile (orange), and combined (green) failure modes.

spectrometer (Cora 5001 DUAL, Anton Paar Switzerland AG, Buchs, Switzerland) equipped with a 785 nm laser. Laser power was 200 mW, and spectra were acquired within five seconds and averaged over three measurements. The ~25 mm long diaphysis sections where the bone rods were extracted initially (Fig. 1) were positioned on the manually adjustable XY stage. The Z position of the sample was adjusted to match the setups' focal plane. Two measurements were performed within an area of ~4 mm^2 on either side of the extraction locations on the proximal site, resulting in 4 spectra per sample. Prior to the measurements, the absence of the thermal effects from the long-term laser exposure were checked by collecting the time series of spectra at described parameters. Spectra processing was done in Python (version 3.11.4) (Van Rossum and Drake, 2009). All spectra were background-subtracted (second-order polynomial fit for local minima) and corrected for cosmic rays (Anton Paar instrument software v1.4 in-build function) while no smoothing was applied. Peaks of interest representing mineral and collagen content were further fit with the Lorentzian function superposition using a least square scheme (scipy.optimize.leastsq) (Kochetkova et al., 2022, 2021). The ratio of the secondary phosphate (v_2PO_4, 410–460 cm^{-1}) over the amide III (1215–1300 cm^{-1}) bands was used as an indirect estimation of the bone mineralization level, as suggested by Roschger et al. (Roschger et al., 2014). Both peaks were fitted with a double Lorentzian function using a least-square scheme, and the ratio of the integral areas provided the mineral-to-matrix ratio (ρ_{MM}). Crystallinity (X_c) was defined as the inverse value of the v_1PO_4 peak full width at half maximum (Akkus et al., 2003; Morris and Mandair, 2011; Yerramshetty and Akkus, 2008). The intensity ratio of the amide I sub-bands $I_{\sim1660}/I_{\sim1683}$ and $I_{\sim1670}/I_{\sim1640}$ provided the matrix maturity ratio and collagen disorder/order ratio, respectively (Unal et al., 2021, 2019). The matrix maturity ratio was considered as a non-quantitative measure of cross-link maturity (McNerny et al., 2015; Unal et al., 2021), while the collagen disorder/order ratio was related to the disorderliness in collagen helical structure, as was demonstrated through mechanical and thermal denaturation of bone (Unal et al., 2016).

2.9. Statistical analysis

Statistical analysis was conducted by performing simple and multiple linear regressions using the statsmodels package from Python 3.11 (Van Rossum and Drake, 2009). Analysis of covariance (ANCOVA) was used to explore the effects of sex and age on several mechanical variables. Significance was assigned to $p < 0.05$. For each variable, the mean ± standard deviation was reported. The coefficient of variation (CV) was defined as the ratio of the standard deviation to the mean.

3. Results

Descriptive statistics of the assessed morphological, compositional, and mechanical parameters and correlation coefficients along with significance levels are indicated in Tables 1 and 2, respectively. Since analyses show that all variables but ρ, WF_m, E_m^{app}, and Collagen Disorder/Order Ratio were not significantly different between females and males ($p > 0.05$) the data was pooled.

3.1. Gravimetric measures

On average, samples exhibited the highest weight fractions of mineral (58.7 ± 1.3 %), followed by organic fraction (34.9 ± 0.9 %). Water weight fraction was the lowest for the investigated samples (6.3 ± 1.6 %), whilst exhibiting the highest variation (CV = 0.253). A correlation to age at death could only be found for WF_m ($r = -0.24$, $p < 0.05$) but neither for WF_o nor WF_w (Table 2).

3.2. Morphological measures

Samples exhibited mean ρ and TMD of 93.2 ± 5.1 % and 1114.0 ± 18.6 mg HA/cm^3, respectively (Table 1). Neither ρ nor TMD were dependent on age at death. Instead, mineral-related characteristics of samples demonstrated strong positive correlation between the measurement techniques (Fig. 4). TMD was found to be positively related to WF_m ($r = 0.58$, $p < 0.001$), but also to ρ_{MM} ($r = 0.36$, $p < 0.01$). Similarly, ρ_{MM} positively correlated with WF_M ($r = 0.36$, $p < 0.001$).

3.3. Raman measures

Contrary to gravimetric measurements, Raman spectroscopy allowed to assess relative bone composition in a non-destructive manner. Relative mineral and organic bone properties were measured, where mineral crystallinity (X_c) and mineral-to-matrix ratio (ρ_{MM}) exhibited values of 0.68 ± 0.05 and 0.064 ± 0.0004, respectively. Collagen properties, as extracted from the amide I sub-peak ratios, included collagen disorder/order ratio (1.44 ± 0.05) and matrix maturity ratio (1.45 ± 0.06) (Table 1). A significant but weak correlation was found between collagen disorder/order ratio and age at death ($r = 0.25$, $p < 0.05$). Other compositional properties did not correlate with the donor's age at death (Table 2).

Relative mineral and organic bone properties correlated with the gravimetric measurements. In particular, ρ_{MM} positively correlated with WF_m ($r = 0.36$, $p < 0.001$) (Fig. 4), while X_c negatively correlated with WF_o ($r = -0.26$, $p < 0.05$). Collagen disorder/order ratio positively

Table 1
Descriptive statistics of the entire sample population of different types of tests' morphological, compositional, and mechanical parameters for pooled, male, and female data; I: μCT and mechanical testing; II: gravimetry; III: Raman spectroscopy. Significant values are shown in bold indicated with an asterisk.

Type of test	Variable	Symbol	Unit	Pooled		Female		Male		p-Value
				n	Mean ± std	n	Mean ± std	n	Mean ± std	
	Age	–	yrs	79	81 ± 9	45	82 ± 9	34	80 ± 9	0.277
I	Bone Volume Fraction	ρ	%	76	93.2 ± 5.08	42	92.2 ± 4.97	34	95.0 ± 3.14	**0.005***
	Tissue Mineral Density	–	mg/cm^3	76	1114.1 ± 18.6	42	1111.0 ± 15.6	34	1117.8 ± 21.5	0.114
	Apparent Modulus Mineralized	E_m^{app}	GPa	73	15.6 ± 1.86	40	15.2 ± 1.85	33	16.2 ± 1.64	**0.025***
	Modulus Mineralized	E_m	GPa	73	16.7 ± 1.69	40	16.5 ± 1.55	33	17.1 ± 1.85	0.170
	Ultimate Apparent Stress	σ_u^{app}	MPa	70	14.9 ± 4.8	39	14.8 ± 5.1	31	15.3 ± 4.3	0.671
	Ultimate Strain	ϵ_u	%	70	8.1 ± 1.2	39	8.0 ± 1.2	31	8.2 ± 1.1	0.430
	Apparent Modulus Demineralized	E_o^{app}	MPa	70	198.6 ± 38.7	39	199.6 ± 38.7	31	199.1 ± 38.6	0.956
	Modulus Demineralized	E_o	MPa	70	214.1 ± 42.9	39	217.4 ± 42.9	31	210.6 ± 43.8	0.516
II	Mineral Weight Fraction	WF_m	%	79	58.7 ± 1.31	45	58.4 ± 1.04	34	59.1 ± 1.51	**0.026***
	Organic Weight Fraction	WF_o	%	79	34.9 ± 0.86	45	35.0 ± 0.87	34	34.9 ± 0.86	0.654
	Water Weight Fraction	WF_w	%	79	6.3 ± 1.61	45	6.5 ± 1.38	34	6.0 ± 1.84	0.124
III	Mineral-to-Matrix Ratio	ρ_{MM}	–	79	0.6770 ± 0.0457	45	0.677 ± 0.0458	34	0.678 ± 0.0468	0.878
	Crystallinity	X_c	–	79	0.0641 ± 0.0004	45	0.0642 ± 0.0004	34	0.0641 ± 0.0004	0.213
	Collagen Disorder/Order Ratio	–	–	79	1.4420 ± 0.0497	45	1.4538 ± 0.0522	34	1.4254 ± 0.0418	**0.011***
	Matrix Maturity Ratio	–	–	79	1.4470 ± 0.0615	45	1.4581 ± 0.0650	34	1.4334 ± 0.0552	0.079

Table 2
Pearson correlation coefficients between investigated properties obtained by simple linear regression. Significant values are shown in bold. Levels of significance are: * ($p < 0.05$), ** ($p < 0.01$), *** ($p < 0.001$).

	Age	ρ	*TMD*	E_m^{app}	E_m	E_o^{app}	E_o	σ_u^{app}	ϵ_u	WF_m	WF_o	WF_w	ρ_{MM}	X_c	*CDO*
ρ	−0.20														
TMD	−0.08	**0.28***													
E_m^{app}	**−0.32****	**0.55*****	0.22												
E_m	**−0.28***	0.11	0.11	**0.89****											
E_o^{app}	−0.20	0.04	**−0.37****	**0.49*****	**0.56*****										
E_o	−0.14	**−0.25***	**−0.43*****	**0.31****	**0.51*****	**0.96*****									
σ_u^{app}	−0.19	**0.27***	**−0.31****	**0.58*****	**0.55*****	**0.76*****	**0.65*****								
ϵ_u	−0.07	0.30*	−0.12	**0.39*****	**0.29***	0.19	0.09	**0.73*****							
WF_m	**−0.24***	**0.43*****	**0.58*****	**0.47*****	**0.32****	−0.14	**−0.26***	−0.01	0.09						
WF_o	0.16	0.04	**−0.30***	−0.17	−0.21	−0.01	−0.02	0.05	0.08	0.06					
WF_w	0.10	**−0.38*****	**−0.32****	**−0.29***	−0.15	0.12	0.22	−0.02	−0.12	**−0.84*****	**−0.58*****				
ρ_{MM}	−0.22	0.18	**0.36****	**0.35****	**0.32****	0.06	0.01	−0.01	−0.04	**0.36*****	−0.19	−0.19			
X_c	−0.16	−0.06	0.18	−0.01	0.02	−0.14	−0.13	−0.08	−0.03	0.09	**−0.26***	0.06	0.01		
CDO	**0.25***	−0.09	−0.04	**−0.23***	−0.23	−0.12	−0.09	−0.19	−0.10	−0.11	**0.3****	−0.07	**−0.26***	**−0.28***	
MMAT	0.01	−0.09	−0.20	−0.08	−0.06	−0.04	−0.03	−0.01	−0.01	−0.12	−0.155	0.18	**−0.23***	0.11	−0.02

Key: ρ, bone volume fraction; TMD, tissue mineral density; E_m^{app}, apparent Young's modulus (native); E_m, Young's modulus (native); E_o^{app}, apparent Young's modulus (demineralized); E_o, Young's modulus (demineralized); σ_u^{app}, apparent ultimate stress; ϵ_u, ultimate strain; WF_m, mineral weight fraction; WF_o, organic weight fraction; WF_w, water weight fraction; ρ_{MM}, mineral-to-matrix ratio; X_c, crystallinity; CDO, collagen disorder/order ratio; MMAT, matrix maturity ratio.

correlated with WF_o ($r = 0.3$, $p < 0.01$). Mineralization related characteristics were found to correlate between the μCT and Raman spectroscopy measurements. In particular, ρ_{MM} positively correlated with TMD ($r = 0.36$, $p = 0.001$) (Fig. 4).

3.4. Mechanical measures

Young's modulus of the mineralized phase on the intrinsic E_m and apparent E_m^{app} level exhibited values of 16.7 ± 1.69 GPa and 15.6 ± 1.86 GPa. Significant negative correlations were found between age at death and E_m ($r = -0.28$, $p < 0.05$) and age at death and E_m^{app} ($r = -0.32$, $p < 0.001$). When related to compositional metrics, both E_m and E_m^{app} show a significant positive correlation with WF_m and ρ_{MM}. At the same time, a similar trend is evident between E_m^{app}, and ρ ($r = 0.55$, $p < 0.001$) and between E_m^{app}, and E_m ($r = 0.89$, $p < 0.001$).

As far as the mechanical properties of the organic matrix are concerned, E_o and E_o^{app} exhibit mean values of 214.1 ± 42.9 MPa and 198.8 ± 38.7 MPa while ultimate apparent stress σ_u^{app} and ultimate strain ϵ_u reached values of 14.9 ± 4.8 MPa and 8.1 ± 1.2 %, respectively (Table 1). In contrast to mineralized properties, none of those metrics correlate with age at death. Ultimate stress of the organic phase, defined as the division of maximum stress by the organic area, presented no correlations with any metrics and, therefore, was not included in Table 2.

Significant positive correlations between E_o^{app}, and E_m ($r = 0.56$, $p < 0.001$), and E_o^{app} and E_m^{app} ($r = 0.49$, $p < 0.001$) were identified. With regards to ultimate properties, σ_u^{app} shows correlations with mechanical properties of both native and demineralized samples on the intrinsic and apparent level, such as E_m ($r = 0.55$, $p < 0.001$), E_m^{app} ($r = 0.58$, $p < 0.001$) but also E_o ($r = 0.65$, $p < 0.001$), and E_o^{app} ($r = 0.76$, $p < 0.001$) (Fig. 6). Finally, ϵ_u shows significant positive correlations with E_m ($r = 0.29$, $p < 0.05$), E_m^{app} ($r = 0.39$, $p < 0.001$), and σ_u^{app} ($r = 0.73$, $p < 0.001$) (Fig. 6). Interestingly, no correlations between ϵ_u and Young's moduli of the organic phase on both intrinsic and apparent levels could be observed.

3.5. Morpho-mechanical measures

With regards to the relation between the native sample morphology and mechanical properties of demineralized samples, it was found that σ_u^{app} exhibits correlations with both ρ ($r = 0.27$, $p < 0.05$) and TMD ($r = -0.31$, $p < 0.01$). Similar behavior can be observed between ϵ_u and ρ ($r = 0.3$, $p < 0.05$). Furthermore, a weak negative correlation was found between E_o and WF_m ($r = -0.26$, $p < 0.05$), E_o and TMD ($r = -0.43$, $p < 0.001$), and E_o and ρ ($r = -0.25$, $p < 0.05$) (Fig. 7). Stronger correlations were evident between E_o and TMD ($r = -0.43$, $p < 0.001$) and E_o and E_m ($r = 0.51$, $p < 0.001$) (Fig. 5). On the apparent level, the correlation between E_{oc}^{app}, and WF_m vanishes but remains significant between E_{oc}^{app}, and TMD ($r = -0.31$, $p < 0.01$).

4. Discussion

Specimens of 44 individuals aged 57 to 96 years at death were tested at the macroscale in native and demineralized states utilizing uniaxial tension testing. Specimen-specific morphological parameters were measured using μCT and gravimetry. The chemical composition was investigated by Raman spectroscopy. Statistical analyses between mechanical properties, morphological, and chemical properties were performed to better understand the structure-mechanical property relationships of the organic phase and particularly collagen type I in compact bone.

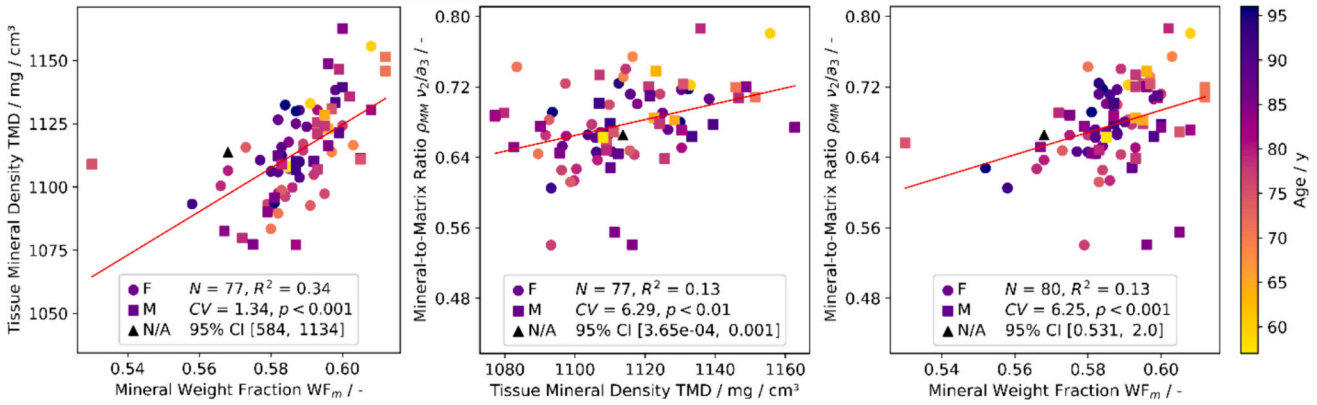

Fig. 4. Correlation of morphological and compositional properties assessed with μCT (TMD), Raman spectroscopy (ρ_{MM}), and gravimetry (WF_m) on different samples (Table 1) showing consistency of mineral content assessment.

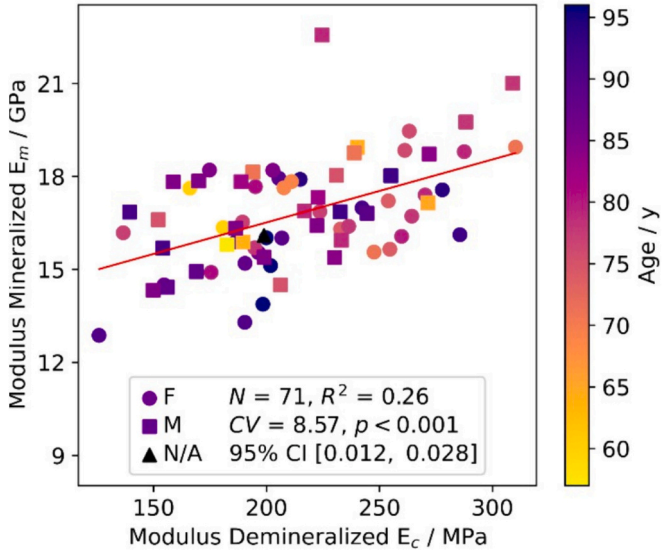

Fig. 5. Statistically significant positive correlation of elastic moduli of native and demineralized samples.

4.1. Influence of donor age at death

4.1.1. Compositional properties

WF_m showed good agreement with findings of Wang et al. (Wang et al., 2002). WF_m showed a significant but weak age dependence ($r = -0.24$, $p < 0.05$) which is again in line with findings of Wang et al. (Wang et al., 2002), who found a significantly lower WF_m for a middle-aged (50–69 years) and an elderly group (> 70 years) when compared to a young (19–49 years) cohort. However, the significance was lost when comparing the middle-aged to the elderly group, to which the donor age at death range of the present study corresponds. While several studies report relative mineral content to be independent of age (Boivin and Meunier, 2002; McCalden et al., 1993; Mirzaali et al., 2016), recent work done by Bonicelli et al. (Bonicelli et al., 2022) showed an age dependent increase of relative mineral content until the age of approximately 35 years, while remaining at a constant level from 35 years onwards. Thus, it is believed that the occurrence of this weak age dependency of WF_m can be attributed to a sampling effect, considering the range of the donor age at death of the present study.

Organic weight fraction WF_o exhibited no age dependence, which is again in line with findings of Wang et al. (Wang et al., 2002). In contrast, Saito et al. (Saito, 1999) found a significant age dependence of total collagen content for several anatomical locations in a cohort of 40 healthy male subjects aged 0 months to 84 years of age. This age dependency might be lost when considering only subjects in an age range similar to this study, as the peak collagen content is reached between 10 and 20 years of age and afterward rapidly decreases until the age of 50 years (Saito, 1999). The same applies for the study of Bonicelli et al. (Bonicelli et al., 2022) where again a significant decrease of relative organic weight was observed until the age of approximately 35 years, but no significant change from 35 years onwards.

Water weight fraction WF_w showed a relatively high standard deviation, probably caused by the lacking ability of water to escape the porous network during centrifugation. WF_w correlates significantly with WF_m but not with WF_o, suggesting that minerals and water share the

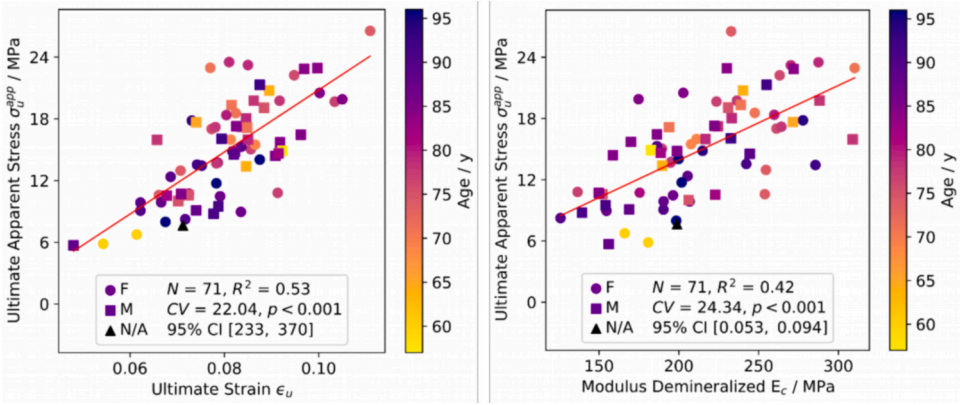

Fig. 6. Statistically positive significant correlations between mechanical properties of demineralized samples.

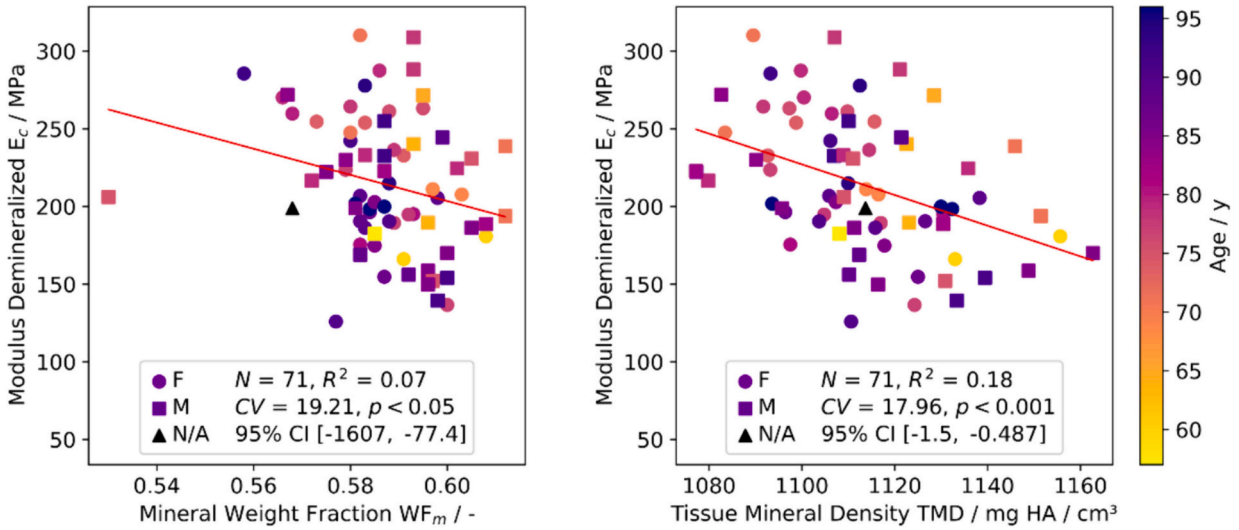

Fig. 7. Weak but statistically significant negative correlations between modulus of demineralized bone (E_o) and compositional properties.

volume among each other.

A fiber-optic Raman spectrometer was used to assess local relative bone composition. In contrast to laboratory based micro spectrometers, fiber-optic Raman is more flexible with regard to the sample geometry and provides generally larger spot size (mm-range versus μm-range), allowing measuring and correlating bone properties at the apparent level. However, the presented compositional properties were averaged from the local measurements. Acquired values of the relative bone composition were generally in line with previous studies on Raman micro spectrometers: 0.4–1.6 mineral-to-matrix ratio (Kochetkova et al., 2023; Roschger et al., 2014), 0.05–0.06 mineral crystallinity (Kochetkova et al., 2023; Mirzaali et al., 2016; Yerramshetty and Akkus, 2008), 1.35–1.60 collagen disorder/order ratio (Unal et al., 2019, 2016), 1.40–1.47 matrix maturity ratio (Kochetkova et al., 2023).

Raman spectroscopy showed that ρ_{MM}, X_c, and matrix maturity ratio did not vary with donor age at death. With respect to ρ_{MM}, this confirms results gathered by Kochetkova et al. (Kochetkova et al., 2023). Other ρ_{MM} Raman band ratios (v_1PO_4/amide I) were also shown to be independent of donor age at death (Boivin and Meunier, 2002; Gamsjaeger et al., 2014; Mirzaali et al., 2016; Unal et al., 2019). A similar absence of correlation with the donor's age at death for X_c is in line with other studies (Kochetkova et al., 2023; Makowski et al., 2015; Mirzaali et al., 2016). In contrast to our observations ($r = 0.01$, $p > 0.05$), the matrix maturity ratio is expected to increase with age, following available studies (Kochetkova et al., 2023; Unal et al., 2019). However, we have a narrower range of the donor's age at death, which may diminish potential correlation. The collagen disorder/order ratio is also expected to increase with the higher age (Unal et al., 2019), which is in line with our findings ($r = 0.25$, $p < 0.05$).

We observed a strong correlation between the mineral and organic bone fractions as assessed via Raman spectroscopy, gravimetric analysis, and micro-CT. As anticipated, a positive correlation between ρ_{MM} and WF_m is observed ($r = 0.36$, $p < 0.001$), in line with findings of Taylor et al. (Taylor et al., 2017). To our knowledge, this is the first study where Raman crystallinity and collagen disorder/order ratio were correlated with the bone weight fractions. We observed increasing WF_o with decreasing X_c ($r = -0.26$, $p < 0.05$), which can be due to the limited available space for the mineral growth, which is otherwise occupied by the proteins (collagen and non-collagenous) and water (Lees, 1987). What is more, we observe a positive correlation between ρ_{MM} and TMD ($r = 0.36$, $p < 0.01$), as assessed via μCT, which is in line with a study of Indermaur et al. (Indermaur et al., 2021). We moreover observed some cross-correlations within the Raman ratios. For example, ρ_{MM} negatively correlates with collagen disorder/order ratio ($r = -0.26$, $p < 0.05$) and matrix maturity ratio ($r = -0.23$, $p < 0.05$). This is, however, due to the Raman ratio's quantification similarities since all of these Raman parameters depend on the amide III integral area.

4.1.2. Morphological properties

From the morphological analysis, microstructural properties such as ρ and TMD were calculated. Values for ρ and TMD are in accordance with results of several studies (Eneh et al., 2016; Mirzaali et al., 2016; Tassani et al., 2011; Wang et al., 2002). However, ρ was higher as in McCalden et al. (McCalden et al., 1993), where certain female specimens showed values of 0.7 in specimens obtained from the mid-diaphyseal region. Neither ρ nor TMD significantly correlated with age although a negative trend is present, which aligns with findings by Wang et al. (Wang et al., 2002) if compared to the same age range as for the cohort in this study. This contrasts earlier but also recent results (Bonicelli et al., 2022; Malo et al., 2013; McCalden et al., 1993; Zioupos, 2001), where an age dependency of porosity has been demonstrated. The low number of donors with a younger age of death than 60 years could explain a missing age dependency of ρ.

4.1.3. Mechanical properties

Macromechanical properties such as elastic modulus of the native and demineralized compact bone samples and ultimate stress and strain of the demineralized samples are well comparable to the literature (Carter et al., 1981; Catanese III et al., 1999; Jepsen et al., 1999; Kotha and Guzelsu, 2003; Mirzaali et al., 2016; Pattin et al., 1996; Reilly et al., 1974; Reilly and Burstein, 1975; Wang et al., 2002; Zioupos and Currey, 1998). E_m and E_m^{app} are significantly correlated to age, while E_o, E_o^{app}, and ϵ_u are not. These findings are in contrast to results obtained by Wang et al. (Wang et al., 2002), who found an age dependency for σ_u and E_o but not for ϵ_u and E_m, respectively. However, the dependence of E_m on the age of the individual is attributed to the decreasing trend in mineralization that is observed with age.

4.2. Consistency between measurement techniques

Relating TMD, ρ_{MM}, and WF_m with each other yields significant correlations (Fig. 4), whereas the most substantial dependence is found between TMD and WF_m ($r = 0.58$, $p < 0.001$) as those quantities were evaluated on the complete sample volume, although on different samples. ρ_{MM} with TMD ($r = 0.36$, $p < 0.01$) and ρ_{MM} with WF_m ($r = 0.36$, $p < 0.001$) exhibit weaker but significant correlations since the analysis of ρ_{MM} was performed on a volume of approximately 1 mm^3 at adjacent locations (Fig. 1). However, due to bone heterogeneity, it is obvious to

find weaker correlations between those techniques when not measuring on the same samples. Additionally, the range of mineralization is quite narrow, since only bone samples of skeletally mature donors were explored. That contrasts with other studies, which focused on the calibration between such techniques (Taylor et al., 2017), where chemical standards with a wide range of mineralization were used, reaching R^2 values of up to 0.99. Such calibration was outside the scope of the current study, but the correlation analysis was rather used to compare the complementary information about the mineral fraction between the techniques. The presence of such correlations suggests that those methods are complementary for cortical bone mineral content estimation.

While being first employed over a 150 years ago, gravimetric analysis provides the oldest, yet simplest approach of destructive bone composition analysis. It has faced drastic improvements in the past decades e.g., increasing accuracy and precision of weighing techniques and equipment. It is capable of measuring absolute mineral, organic and water weight of bone specimens by pyrolyzing water and organic components at different temperature levels, while yielding best results for mineral and organic weight. Assessment of water weight has been shown less viable, due to the porous nature of bone tissue rendering the definition of a wet state difficult. This fact is reflected in the CV of the mineral, organic, and water weight fraction of the present work, which show values of 0.022, 0.025, and 0.253, respectively. Suitable techniques for analysis of the water compartment of bone are nuclear magnetic resonance (NMR) spectroscopy and perhaps dynamic vapor sorption (DVS). NMR is a non-destructive method where ^{1}H and ^{31}P isotopes are brought to resonance by applying a strong magnetic field at different frequencies, which depend on the local chemical environment (Wehrli and Fernández-Seara, 2005). The relative pore water content of bone is then quantified from the ^{1}H spectra and has been shown to be a surrogate measure for cortical porosity (Fernández-Seara et al., 2004) while also being correlated with mechanical properties (Bae et al., 2014; Granke et al., 2015; Nyman et al., 2008). In contrast to NMR and similar to the gravimetric technique used in this study, DVS is a destructive method. It measures vapor sorption under controlled relative humidity and temperature. By determination of the sorption isotherm for each humidity value, the corresponding water content at a constant temperature can be estimated (Grönquist et al., 2019; Peruzzi et al., 2021). In contrast to the technique used in this study, achieving a reproducible wet state in a short amount of time is an advantage of DVS.

As the gold standard technique to visualize three dimensional bone morphology at the microstructural scale, μCT is employed to estimate relative tissue mineralization based on calibrated grey value images (Rüegsegger et al., 1996). On the other hand, Raman spectroscopy is used to study the chemical composition and bonding environments of mineral and organic tissue constituents, by associating the frequency difference of an incident and emergent beam to the molecule's unique vibrational spectra (Bazin et al., 2009). While μCT can be phantom-calibrated and thus providing quantitative information on mineralization, Raman spectroscopy yields qualitative data. Although there is a possibility to calibrate ρ_{MM} with mineral content, it is a time-consuming task, especially when done for every Raman derived parameter (Roschger et al., 2014). However, Raman spectroscopy provides information on both mineral and organic weight fraction allowing to cumulatively access bone composition. Combining μCT and Raman spectroscopy renders accessing both bone quantity (bone mass) and quality.

4.3. Morpho-mechanical relationships

Multiple linear regression was performed while E_m was used as the dependent variable and WF_m and age as the explanatory variables. The results indicated a dominant influence of WF_m on E_m ($p < 0.01$), but age remains significant ($p < 0.05$). Similarly, when E_m^{app} is set as the dependent variable and ρ, WF_m, and age as explanatory variables, ρ contributes the most ($p < 0.001$) while WF_m and age both remain significant ($p < 0.05$).

Interestingly, E_m was found to correlate significantly with E_o ($r = 0.51$, $p < 0.001$), indicating that the organic matrix affects the composites' mechanical properties independently of collagen quantity. This suggests that the stiffening and strengthening effect of collagen connectivity is preserved from the small strains in the native condition to the much larger strains in the demineralized condition.

Apparent elastic moduli were found to significantly correlate with the corresponding intrinsic moduli, as those intrinsic properties were normalized by ρ.

With respect to the native bone tissue, E_m^{app} was found to correlate with ρ because both metrics contain A_{app}. Significant correlation was obtained between E_m^{app}, and ρ_{MM} but also E_m^{app}, and WF_m, which has been shown extensively in the past (Courtney et al., 1996; Indermaur et al., 2021; Leng et al., 2009; Martin, 1993; Martin et al., 1985; Zioupos and Currey, 1998). On the intrinsic level, interestingly, E_m did not correlate with TMD, although correlations between E_m and WF_m, E_m and ρ_{MM}, TMD and WF_m, and TMD and ρ_{MM} exist. This may be due to the narrow age range of the individuals and the narrow range of mineralization, as mentioned earlier.

E_o correlates negatively and significantly with both TMD ($r = -0.43$, $p < 0.001$), ρ ($r = -0.25$, $p < 0.05$), and WF_m ($r = -0.26$, $p < 0.05$) (Fig. 7), indicating that a reduced mineral content leads to a stiffening of the collagen fibers which is consistent with computational models of the bone ECM (Alizadeh et al., 2020). A reduced number of mineral-collagen connections may cause such an effect, whereas the lack of extrafibrillar and intrafibrillar mineral crystals could induce a loss of waviness leading to a collagen fiber pre-stretch that manifests in a stiffer response. As previously mentioned, the correlation between E_o and WF_m is weaker than between E_o and TMD, due to E_o and WF_m being evaluated on different samples and because of the dependency of WF_m on WF_w.

Relative bone composition measured via Raman spectrometry demonstrated some marginal correlation with the measured tensile bone properties. ρ_{MM} correlated positively with E_m^{app} ($r = 0.35$, $p < 0.01$). This is in line with the site-matched measurements carried on Raman microspectroscopy and nanoindentation (Indermaur et al., 2023, 2021; Kochetkova et al., 2023). A matching negative correlation was observed between X_c vs. elastic moduli and collagen disorder/order ratio vs. E_m^{app} (for both $r = -0.23$, $p < 0.05$), suggesting a hidden interplay of the mineral and organic bone fraction into the output bone mechanical properties.

A property that has not been investigated in this study, is collagen fiber orientation (CFO). Martin et al. (Martin and Ishida, 1989) investigated the effect of CFO, porosity, density, and mineralization on cortical bone strength, and found that CFO presented the best predictor of tensile strength for bovine plexiform ($r = 0.480$, $p = 0.002$) and osteonal ($r = 0.628$, $p = 0.021$) bone.

4.4. Limitations

This study has several limitations. First, the donors' medication history, lifestyle, and disease state were unknown, which may lead to biased results due to changes in composition or macro- and microstructural deterioration caused by the factors mentioned above. Furthermore, anatomical specimens used for this study were taken from individuals at a relatively high mean age of death of 81 years and a rather narrow age range of 57 to 96 years. That contrasts with another study (Wang et al., 2002), which included donor material from young donors (19–49 years of age), leading to an age-dependent decrease of collagen and mineral strength compared to the elderly (>70 years of age). Hence, the correlation among mechanical, morphological, and compositional properties in the present study yields weaker results since age-related changes are less prominent than in younger cohorts,

showing a broader age distribution.

Bone is an anisotropic, viscoelastic composite material consisting of hydroxyapatite-reinforced collagen fibrils with varying orientations. Thus, age-related changes in the collagen network might be orientation-dependent and have different effects on the mechanical behavior of bone in other orientations. However, in this study, only longitudinal tensile properties of bone and the organic phase were measured. Thus, the results of the present work are limited in this respect. However, it is assumed that transverse tensile properties, in contrast to longitudinal properties, may be decreased.

The tensile testing procedure used in this work does not imitate physiological conditions but is artificial. The collagen network is located within the mineral matrix and consists of spiral-shaped collagen fibers oriented in various directions inside old and newly formed osteons. Cross-links connect these collagen structures to the mineral matrix at a random occurrence. By demineralization, the mineral phase that provides stiffness and strength to the bone and prevents excessive deformation is removed. The collagen fibers can no longer attach to the mineral matrix and might be unconnected, solely attached to each other. However, the effects of demineralization on enzymatic and non-enzymatic cross-links as well as to other organic components of the bone matrix were not investigated. Thus, while the collagen network within the mineral matrix accomplishes its function perfectly, altered mechanical properties are presented for both, native bone (Casari et al., 2021; Gustafsson et al., 2018) and non-mineralized collagen fibrils (Masic et al., 2015; Ping et al., 2022) when separated from each other. Investigating the deformation of mineral and collagen in bone by combining in situ testing of fibrolamellar bone with simultaneous SAXS and WAXD measuring tissue, fibrillar, and mineral strain of single fibrolamellar bone packets in a tensile testing setup revealed approximately constant fibril-to-tissue (0.41) and mineral-to-tissue (0.16) strain ratio in the elastic response (yield strain = 0.91 %) (Gupta et al., 2006). This may be an indication that testing of non-mineralized collagen is valid as a similar mechanical behavior may be present in the absence of mineral. However, reduced mechanical properties are captured with the present experimental setup. Additionally, the effect of the presence of mineral at both ends of the demineralized tensile specimens on organic tensile properties remains unknown. However, since failure always occurred in the region of the gauge section, it is believed, that there is only minor influence of such boundary effects.

The cross-sectional area of tensile test specimens was not measured after demineralization or during the loading process. Instead, the original cross-section measured by μCT was used to calculate nominal (or engineering) stresses in both experiments. While the small strain assumption holds true for loading of native samples, it does not for loading of demineralized samples, which implies that the nominal stress diverges from Cauchy stress in the latter case.

Two cortical bone rods from the proximal lateral aspect were extracted per femur while one sample was tested by gravimetric techniques, and the other one was employed for μCT imaging and mechanical testing. Additionally, Raman spectroscopy was performed on the remaining bone sections. Finally, the results of those three analyses routes were compared, assuming similar mechanical, morphological, and compositional characteristics. Although measurement locations were close to each other, differences might exist due to the heterogeneous nature of bone. Furthermore, as mentioned previously, the range of mineralization is relatively narrow, since only bone samples of skeletally mature donors were explored. Using chemical standards with a wide range of mineralization to calibrate those techniques, could have been beneficial to reach much better correlations. However, such calibration was outside the scope of the current study, but the correlation analysis was rather used to compare the complementary information about the mineral fraction between the techniques.

As noted earlier, collagen cross-links such as enzymatic cross-links and AGEs may have an impact on several mechanical properties of collagen fibrils and the collagen-mineral composite structure as pointed out in the past (Knott et al., 1995; Opsahl et al., 1982; Oxlund et al., 1995). However, this study did not include quantification of those chemical components, hence their influence on mechanical properties remains elusive.

Due to the design of this study, the post-yield mechanical behavior of the native samples could not be tested. Relation of post-yield properties to morphological parameters may have contributed to a better understanding of the organic-mineral interplay in cortical bone.

5. Conclusion

This study, consisting of macro-tensile tests in hydrated condition and μCT on the same mineralized and demineralized cortical bone specimens, gravimetry, and Raman spectroscopy, revealed that the age range is too narrow to find a significant decrease of volume fraction, and mechanical properties with age at death as shown in previous studies, although the trends are present. Furthermore, the mechanical properties of demineralized bone do not depend on the original volume fraction. Both the organic and mineral fractions of bone are significant determinants of mineralized bone stiffness whereas an increase in the mineral fraction decreases the stiffness and strength of the organic phase which is consistent with computational models of the bone ECM. As suggested by some weak correlations, compositional, morphological, and mechanical properties must imperatively be measured on the same volumes.

This study only focuses on whole organ age but not on tissue age. Thus, it would be interesting to assess the tissue age of cortical bone, i.e., by analyzing cement lines and their density, which could provide valuable insight into mineral-collagen and collagen-collagen interactions.

CRediT authorship contribution statement

Stefan Bracher: Writing – original draft, Visualization, Validation, Software, Methodology, Investigation, Formal analysis, Data curation. **Benjamin Voumard:** Writing – review & editing, Validation, Software, Methodology. **Mathieu Simon:** Writing – review & editing, Validation, Software. **Tatiana Kochetkova:** Writing – review & editing, Validation, Software, Investigation, Formal analysis. **Michael Pretterklieber:** Writing – review & editing, Resources. **Philippe Zysset:** Writing – review & editing, Validation, Supervision, Resources, Funding acquisition, Conceptualization.

Declaration of competing interest

None.

Data availability

Data will be made available on request.

Acknowledgments

This work was supported by the Swiss National Science Foundation (grant 200365). The authors would like to thank Urs Rohrer and the MDP team for machining mechanical parts needed for the experiments. Furthermore, the authors are highly indebted to all voluntary body donators permitting gross anatomical research.

References

Akkus, O., Rimnac, C.M., 2001. Fracture resistance of gamma radiation sterilized cortical bone allografts. J. Orthop. Res. 19, 927–934. https://doi.org/10.1016/S0736-0266(01)00004-3.

Akkus, O., Polyakova-Akkus, A., Adar, F., Schaffler, M.B., 2003. Aging of microstructural compartments in human compact bone. J. Bone Miner. Res. 18, 1012–1019. https://doi.org/10.1359/jbmr.2003.18.6.1012.

Alizadeh, E., Dehestani, M., Zysset, P., 2020. An efficient two-scale 3D FE model of the bone fibril array: comparison of anisotropic elastic properties with analytical methods and micro-sample testing. Biomech. Model. Mechanobiol. 19, 2127–2147. https://doi.org/10.1007/s10237-020-01328-1.

Consensus development conference: Diagnosis, prophylaxis, and treatment of osteoporosis. Am. J. Med. 94, 1993, 646–650. https://doi.org/10.1016/0002-9343(93)90218-E.

Bae, W.C., Patil, S., Biswas, R., Li, S., Chang, E.Y., Statum, S., D'Lima, D.D., Chung, C.B., Du, J., 2014. Magnetic resonance imaging assessed cortical porosity is highly correlated with μCT porosity. Bone 66, 56–61. https://doi.org/10.1016/j.bone.2014.06.004.

Bailey, A.J., Sims, T.J., Ebbesen, E.N., Mansell, J.P., Thomsen, J.S., Mosekilde, Li, 1999. Age-related changes in the biochemical properties of human cancellous bone collagen: relationship to bone strength. Calcif. Tissue Int. 65, 203–210. https://doi.org/10.1007/s002239900683.

Barth, H.D., Launey, M.E., MacDowell, A.A., Ager, J.W., Ritchie, R.O., 2010. On the effect of X-ray irradiation on the deformation and fracture behavior of human cortical bone. Bone 46, 1475–1485. https://doi.org/10.1016/j.bone.2010.02.025.

Barth, H.D., Zimmermann, E.A., Schaible, E., Tang, S.Y., Alliston, T., Ritchie, R.O., 2011. Characterization of the effects of x-ray irradiation on the hierarchical structure and mechanical properties of human cortical bone. Biomaterials 32, 8892–8904. https://doi.org/10.1016/j.biomaterials.2011.08.013.

Bazin, D., Chappard, C., Combes, C., Carpentier, X., Rouzière, S., André, G., Matzen, G., Allix, M., Thiaudière, D., Reguer, S., Jungers, P., Daudon, M., 2009. Diffraction techniques and vibrational spectroscopy opportunities to characterise bones. Osteoporos. Int. 20, 1065–1075. https://doi.org/10.1007/s00198-009-0868-3.

Boivin, G., Meunier, P.J., 2002. The degree of mineralization of bone tissue measured by computerized quantitative contact microradiography. Calcif. Tissue Int. 70, 503–511. https://doi.org/10.1007/s00223-001-2048-0.

Bonicelli, A., Kranioti, E.F., Xhemali, B., Arnold, E., Zioupos, P., 2022. Assessing bone maturity: compositional and mechanical properties of rib cortical bone at different ages. Bone 155, 116265. https://doi.org/10.1016/j.bone.2021.116265.

Boskey, A.L., Wright, T.M., Blank, R.D., 1999. Collagen and bone strength. J. Bone Miner. Res. 14, 330–335. https://doi.org/10.1359/jbmr.1999.14.3.330.

Britton, M., Parle, E., Vaughan, T.J., 2023. An investigation on the effects of in vitro induced advanced glycation end-products on cortical bone fracture mechanics at fall-related loading rates. J. Mech. Behav. Biomed. Mater. 138, 105619 https://doi.org/10.1016/j.jmbbm.2022.105619.

Burr, D.B., 2002. The contribution of the organic matrix to bone's material properties. Bone 31, 8–11. https://doi.org/10.1016/S8756-3282(02)00815-3.

Burstein, A., Zika, J., Heiple, K., Klein, L., 1975. Contribution of collagen and mineral to the elastic-plastic properties of bone. JBJS 57.

Burton, B., Gaspar, A., Josey, D., Tupy, J., Grynpas, M.D., Willett, T.L., 2014. Bone embrittlement and collagen modifications due to high-dose gamma-irradiation sterilization. Bone 61, 71–81. https://doi.org/10.1016/j.bone.2014.01.006.

Carter, D.R., Caler, W.E., Spengler, D.M., Frankel, V.H., 1981. Fatigue behavior of adult cortical bone: the influence of mean strain and strain range. Acta Orthop. Scand. 52, 481–490. https://doi.org/10.3109/17453678108992136.

Casari, D., Kochetkova, T., Michler, J., Zysset, P., Schwiedrzik, J., 2021. Microtensile failure mechanisms in lamellar bone: influence of fibrillar orientation, specimen size and hydration. Acta Biomater. 131, 391–402. https://doi.org/10.1016/j.actbio.2021.06.032.

Catanese III, J., Iverson, E.P., Ng, R.K., Keaveny, T.M., 1999. Heterogeneity of the mechanical properties of demineralized bone. J. Biomech. 32, 1365–1369. https://doi.org/10.1016/S0021-9290(99)00128-1.

Compston, J.E., McClung, M.R., Leslie, W.D., 2019. Osteoporosis. Lancet 393, 364–376. https://doi.org/10.1016/S0140-6736(18)32112-3.

Courtney, A.C., Hayes, W.C., Gibson, L.J., 1996. Age-related differences in post-yield damage in human cortical bone. Experiment and model. J. Biomech. 29, 1463–1471. https://doi.org/10.1016/0021-9290(96)84542-8.

Currey, J.D., Foreman, J., Laketić, I., Mitchell, J., Pegg, D.E., Reilly, G.C., 1997. Effects of ionizing radiation on the mechanical properties of human bone. J. Orthop. Res. 15, 111–117. https://doi.org/10.1002/jor.1100150116.

Eneh, C.T.M., Malo, M.K.H., Karjalainen, J.P., Liukkonen, J., Töyräs, J., Jurvelin, J.S., 2016. Effect of porosity, tissue density, and mechanical properties on radial sound speed in human cortical bone: radial sound speed in human cortical bone. Med. Phys. 43, 2030–2039. https://doi.org/10.1118/1.4942808.

Feldkamp, L.A., Goldstein, S.A., Parfitt, M.A., Jesion, G., Kleerekoper, M., 1989. The direct examination of three-dimensional bone architecture in vitro by computed tomography. J. Bone Miner. Res. 4, 3–11. https://doi.org/10.1002/jbmr.5650040103.

Fernández-Seara, M.A., Wehrli, S.L., Takahashi, M., Wehrli, F.W., 2004. Water content measured by proton-deuteron exchange NMR predicts bone mineral density and mechanical properties. J. Bone Miner. Res. 19, 289–296. https://doi.org/10.1359/JBMR.0301227.

Ferrari, S., Lippuner, K., Lamy, O., Meier, C., 2020. 2020 recommendations for osteoporosis treatment according to fracture risk from the Swiss Association against Osteoporosis (SVGO). Swiss Med. Wkly. https://doi.org/10.4414/smw.2020.20352.

Gamsjaeger, S., Hofstetter, B., Fratzl-Zelman, N., Roschger, P., Roschger, A., Fratzl, P., Brozek, W., Masic, A., Misof, B.M., Glorieux, F.H., Klaushofer, K., Rauch, F., Paschalis, E.P., 2014. Pediatric reference Raman data for material characteristics of iliac trabecular bone. Bone 69, 89–97. https://doi.org/10.1016/j.bone.2014.09.012.

Garnero, P., 2012. The contribution of collagen crosslinks to bone strength. BoneKEy Reports 1, 182. https://doi.org/10.1038/bonekey.2012.182.

Granke, M., Does, M.D., Nyman, J.S., 2015. The role of water compartments in the material properties of cortical bone. Calcif. Tissue Int. 97, 292–307. https://doi.org/10.1007/s00223-015-9977-5.

Grönquist, P., Frey, M., Keplinger, T., Burgert, I., 2019. Mesoporosity of delignified wood investigated by water vapor sorption. ACS Omega 4, 12425–12431. https://doi.org/10.1021/acsomega.9b00862.

Gupta, H.S., Seto, J., Wagermaier, W., Zaslansky, P., Boesecke, P., Fratzl, P., 2006. Cooperative deformation of mineral and collagen in bone at the nanoscale. Proc. Natl. Acad. Sci. USA 103, 17741–17746. https://doi.org/10.1073/pnas.0604237103.

Gustafsson, A., Mathavan, N., Turunen, M.J., Engqvist, J., Khayyeri, H., Hall, S.A., Isaksson, H., 2018. Linking multiscale deformation to microstructure in cortical bone using in situ loading, digital image correlation and synchrotron X-ray scattering. Acta Biomater. 69, 323–331. https://doi.org/10.1016/j.actbio.2018.01.037.

Indermaur, M., Casari, D., Kochetkova, T., Peruzzi, C., Zimmermann, E., Rauch, F., Willie, B., Michler, J., Schwiedrzik, J., Zysset, P., 2021. Compressive strength of iliac bone ECM is not reduced in osteogenesis imperfecta and increases with mineralization. J. Bone Miner. Res. 36, 1364–1375. https://doi.org/10.1002/jbmr.4286.

Indermaur, M., Casari, D., Kochetkova, T., Willie, B.M., Michler, J., Schwiedrzik, J., Zysset, P., 2023. Tensile mechanical properties of dry cortical bone extracellular matrix: a comparison among two osteogenesis imperfecta and one healthy control iliac crest biopsies. JBMR Plus, e10826. https://doi.org/10.1002/jbm4.10826.

Jepsen, K.J., Davy, D.T., Krzypow, D.J., 1999. The role of the lamellar interface during torsional yielding of human cortical bone. J. Biomech. 32, 303–310. https://doi.org/10.1016/S0021-9290(98)00179-1.

Kling, J.M., Clarke, B.L., Sandhu, N.P., 2014. Osteoporosis prevention, screening, and treatment: a review. J. Women's Health 23, 563–572. https://doi.org/10.1089/jwh.2013.4611.

Knott, L., Whitehead, C.C., Fleming, R.H., Bailey, A.J., 1995. Biochemical changes in the collagenous matrix of osteoporotic avian bone. Biochem. J. 310 (Pt 3), 1045–1051. https://doi.org/10.1042/bj3101045.

Kochetkova, T., Peruzzi, C., Braun, O., Overbeck, J., Maurya, A.K., Neels, A., Calame, M., Michler, J., Zysset, P., Schwiedrzik, J., 2021. Combining polarized Raman spectroscopy and micropillar compression to study microscale structure-property relationships in mineralized tissues. Acta Biomater. 119, 390–404. https://doi.org/10.1016/j.actbio.2020.10.034.

Kochetkova, T., Groetsch, A., Indermaur, M., Peruzzi, C., Remund, S., Neuenschwander, B., Bellon, B., Michler, J., Zysset, P., Schwiedrzik, J., 2022. Assessing minipig compact jawbone quality at the microscale. J. Mech. Behav. Biomed. Mater. 134, 105405 https://doi.org/10.1016/j.jmbbm.2022.105405.

Kochetkova, T., Hanke, M.S., Indermaur, M., Groetsch, A., Remund, S., Neuenschwander, B., Michler, J., Siebenrock, K.A., Zysset, P., Schwiedrzik, J., 2023. Composition and micromechanical properties of the femoral neck compact bone in relation to patient age, sex and hip fracture occurrence. Bone 177, 116920. https://doi.org/10.1016/j.bone.2023.116920.

Kotha, S.P., Guzelsu, N., 2003. Tensile damage and its effects on cortical bone. J. Biomech. 36, 1683–1689. https://doi.org/10.1016/S0021-9290(03)00169-6.

Kuhn, J.L., Goldstein, S.A., Feldkamp, L.A., Goulet, R.W., Jesion, G., 1990. Evaluation of a microcomputed tomography system to study trabecular bone structure. J. Orthop. Res. 8, 833–842. https://doi.org/10.1002/jor.1100080608.

Lees, S., 1987. Considerations regarding the structure of the mammalian mineralized osteoid from viewpoint of the generalized packing model. Connect. Tissue Res. 16, 281–303. https://doi.org/10.3109/03008208709005616.

Leng, H., Dong, X.N., Wang, X., 2009. Progressive post-yield behavior of human cortical bone in compression for middle-aged and elderly groups. J. Biomech. 42, 491–497. https://doi.org/10.1016/j.jbiomech.2008.11.016.

Makowski, A.J., Granke, M., Uppuganti, S., Mahadevan-Jansen, A., Nyman, J.S., 2015. Bone tissue heterogeneity is associated with fracture toughness: a polarization Raman spectroscopy study. In: Choi, B., Kollias, N., Zeng, H., Kang, H.W., Wong, B.J. F., Ilgner, J.F., Nuttal, A., Richter, C.-P., Skala, M.C., Dewhirst, M.W., Tearney, G.J., Gregory, K.W., Marcu, L., Mandelis, A., Morris, M.D. (Eds.), Presented at the SPIE BiOS, San Francisco, California, United States, p. 930341. https://doi.org/10.1117/12.2080350.

Malo, M.K.H., Rohrbach, D., Isaksson, H., Töyräs, J., Jurvelin, J.S., Tamminen, I.S., Kröger, H., Raum, K., 2013. Longitudinal elastic properties and porosity of cortical bone tissue vary with age in human proximal femur. Bone 53, 451–458. https://doi.org/10.1016/j.bone.2013.01.015.

Martin, B., 1993. Aging and strength of bone as a structural material. Calcif. Tissue Int. 53, S34–S40. https://doi.org/10.1007/BF01673400.

Martin, R.B., Ishida, J., 1989. The relative effects of collagen fiber orientation, porosity, density, and mineralization on bone strength. J. Biomech. 22, 419–426. https://doi.org/10.1016/0021-9290(89)90202-9.

Martin, R.B., Burr, D.B., Schaffler, M.B., 1985. Effects of age and sex on the amount and distribution of mineral in Eskimo tibiae. Am. J. Phys. Anthropol. 67, 371–380. https://doi.org/10.1002/ajpa.1330670409.

Masic, A., Bertinetti, L., Schuetz, R., Chang, S.-W., Metzger, T.H., Buehler, M.J., Fratzl, P., 2015. Osmotic pressure induced tensile forces in tendon collagen. Nat. Commun. 6, 5942. https://doi.org/10.1038/ncomms6942.

McCalden, R.W., McGeough, J.A., Barker, M.B., Court-Brown, C.M., 1993. Age-related changes in the tensile properties of cortical bone. The relative importance of changes in porosity, mineralization, and microstructure. JBJS 75.

McNerny, E.M., Gong, B., Morris, M.D., Kohn, D.H., 2015. Bone fracture toughness and strength correlate with collagen cross-link maturity in a dose-controlled lathyrism mouse model. J. Bone Miner. Res. 30, 455–464. https://doi.org/10.1002/jbmr.2356.

Mirzaali, M.J., Schwiedrzik, J.J., Thaiwichai, S., Best, J.P., Michler, J., Zysset, P.K., Wolfram, U., 2016. Mechanical properties of cortical bone and their relationships with age, gender, composition and microindentation properties in the elderly. Bone 93, 196–211. https://doi.org/10.1016/j.bone.2015.11.018.

Morris, M.D., Mandair, G.S., 2011. Raman assessment of bone quality. Clin. Orthop. Relat. Res. 469, 2160–2169. https://doi.org/10.1007/s11999-010-1692-y.

Nguyen, H., Morgan, D.A.F., Forwood, M.R., 2007. Sterilization of allograft bone: effects of gamma irradiation on allograft biology and biomechanics. Cell Tissue Bank. 8, 93–105. https://doi.org/10.1007/s10561-006-9020-1.

Nyman, J.S., Reyes, M., Wang, X., 2005. Effect of ultrastructural changes on the toughness of bone. Micron 36, 566–582. https://doi.org/10.1016/j.micron.2005.07.004.

Nyman, J.S., Roy, A., Tyler, J.H., Acuna, R.L., Gayle, H.J., Wang, X., 2007. Age-related factors affecting the postyield energy dissipation of human cortical bone. J. Orthop. Res. 25, 646–655. https://doi.org/10.1002/jor.20337.

Nyman, J.S., Ni, Q., Nicolella, D.P., Wang, X., 2008. Measurements of mobile and bound water by nuclear magnetic resonance correlate with mechanical properties of bone. Bone 42, 193–199. https://doi.org/10.1016/j.bone.2007.09.049.

Odetti, P., Rossi, S., Monacelli, F., Poggi, A., Cirnigliaro, M., Federici, M., Federici, A., 2005. Advanced glycation end products and bone loss during aging. Ann. N. Y. Acad. Sci. 1043, 710–717. https://doi.org/10.1196/annals.1333.082.

Opsahl, W., Zeronian, H., Ellison, M., Lewis, D., Rucker, R.B., Riggins, R.S., 1982. Role of copper in collagen cross-linking and its influence on selected mechanical properties of chick bone and tendon. J. Nutr. 112, 708–716. https://doi.org/10.1093/jn/112.4.708.

Oxlund, H., Barckman, M., Ørtoft, G., Andreassen, T.T., 1995. Reduced concentrations of collagen cross-links are associated with reduced strength of bone. Bone 17, S365–S371. https://doi.org/10.1016/8756-3282(95)00328-B.

Pattin, C.A., Caler, W.E., Carter, D.R., 1996. Cyclic mechanical property degradation during fatigue loading of cortical bone. J. Biomech. 29, 69–79. https://doi.org/10.1016/0021-9290(94)00156-1.

Peruzzi, C., Ramachandramoorthy, R., Groetsch, A., Casari, D., Grönquist, P., Rüggeberg, M., Michler, J., Schwiedrzik, J., 2021. Microscale compressive behavior of hydrated lamellar bone at high strain rates. Acta Biomater. 131, 403–414. https://doi.org/10.1016/j.actbio.2021.07.005.

Ping, H., Wagermaier, W., Horbelt, N., Scoppola, E., Li, C., Werner, P., Fu, Z., Fratzl, P., 2022. Mineralization generates megapascal contractile stresses in collagen fibrils. Science 376, 188–192. https://doi.org/10.1126/science.abm2664.

Reilly, D.T., Burstein, A.H., 1975. The elastic and ultimate properties of compact bone tissue. J. Biomech. 8, 393–405. https://doi.org/10.1016/0021-9290(75)90075-5.

Reilly, D.T., Burstein, A.H., Frankel, V.H., 1974. The elastic modulus for bone. J. Biomech. 7, 271–275. https://doi.org/10.1016/0021-9290(74)90018-9.

Roschger, A., Gamsjaeger, S., Hofstetter, B., Masic, A., Blouin, S., Messmer, P., Berzlanovich, A., Paschalis, E.P., Roschger, P., Klaushofer, K., Fratzl, P., 2014. Relationship between the v2PO4/amide III ratio assessed by Raman spectroscopy and the calcium content measured by quantitative backscattered electron microscopy in healthy human osteonal bone. J. Biomed. Opt. 19, 065002 https://doi.org/10.1117/1.JBO.19.6.065002.

Rüegsegger, P., Koller, B., Müller, R., 1996. A microtomographic system for the nondestructive evaluation of bone architecture. Calcif. Tissue Int. 58, 24–29. https://doi.org/10.1007/BF02509542.

Saito, M., 1999. Age-related changes in biochemical characteristics of collagen from human weight-bearing and non-weightbearing bone. Tokyo Jikeikai Ika Daigaku Zasshi 327–337.

Saito, M., Marumo, K., 2010. Collagen cross-links as a determinant of bone quality: a possible explanation for bone fragility in aging, osteoporosis, and diabetes mellitus. Osteoporos. Int. 21, 195–214. https://doi.org/10.1007/s00198-009-1066-z.

Saito, M., Marumo, K., Fujii, K., Ishioka, N., 1997. Single-column high-performance liquid chromatographic–fluorescence detection of immature, mature, and senescent cross-links of collagen. Anal. Biochem. 253, 26–32. https://doi.org/10.1006/abio.1997.2350.

Tassani, S., Öhman, C., Baruffaldi, F., Baleani, M., Viceconti, M., 2011. Volume to density relation in adult human bone tissue. J. Biomech. 44, 103–108. https://doi.org/10.1016/j.jbiomech.2010.08.032.

Taylor, E.A., Lloyd, A.A., Salazar-Lara, C., Donnelly, E., 2017. Raman and Fourier transform infrared (FT-IR) mineral to matrix ratios correlate with physical chemical properties of model compounds and native bone tissue. Appl. Spectrosc. 71, 2404–2410. https://doi.org/10.1177/0003702817709286.

Unal, M., Yang, S., Akkus, O., 2014. Molecular spectroscopic identification of the water compartments in bone. Bone 67, 228–236. https://doi.org/10.1016/j.bone.2014.07.021.

Unal, M., Jung, H., Akkus, O., 2016. Novel Raman spectroscopic biomarkers indicate that postyield damage denatures bone's collagen. J. Bone Miner. Res. 31, 1015–1025. https://doi.org/10.1002/jbmr.2768.

Unal, M., Uppuganti, S., Timur, S., Mahadevan-Jansen, A., Akkus, O., Nyman, J.S., 2019. Assessing matrix quality by Raman spectroscopy helps predict fracture toughness of human cortical bone. Sci. Rep. 9, 7195. https://doi.org/10.1038/s41598-019-43542-7.

Unal, M., Ahmed, R., Mahadevan-Jansen, A., Nyman, J.S., 2021. Compositional assessment of bone by Raman spectroscopy. Analyst 146, 7464–7490. https://doi.org/10.1039/D1AN01560E.

Van Rossum, G., Drake, F.L., 2009. Python 3 Reference Manual. CreateSpace, Scotts Valley, CA.

Viguet-Carrin, S., Garnero, P., Delmas, P.D., 2006. The role of collagen in bone strength. Osteoporos. Int. 17, 319–336. https://doi.org/10.1007/s00198-005-2035-9.

Wang, X., Bank, R.A., Tekoppele, J.M., Agrawal, C.M., 2001. The role of collagen in determining bone mechanical properties. J. Orthop. Res. 19, 1021–1026. https://doi.org/10.1016/S0736-0266(01)00047-X.

Wang, X., Shen, X., Li, X., Mauli Agrawal, C., 2002. Age-related changes in the collagen network and toughness of bone. Bone 31, 1–7. https://doi.org/10.1016/S8756-3282(01)00697-4.

Wehrli, F.W., Fernández-Seara, M.A., 2005. Nuclear magnetic resonance studies of bone water. Ann. Biomed. Eng. 33, 79–86. https://doi.org/10.1007/s10439-005-8965-8.

Willett, T.L., Voziyan, P., Nyman, J.S., 2022. Causative or associative: a critical review of the role of advanced glycation end-products in bone fragility. Bone 163, 116485. https://doi.org/10.1016/j.bone.2022.116485.

Yerramshetty, J.S., Akkus, O., 2008. The associations between mineral crystallinity and the mechanical properties of human cortical bone. Bone 42, 476–482. https://doi.org/10.1016/j.bone.2007.12.001.

Zioupos, P., 2001. Ageing human bone: factors affecting its biomechanical properties and the role of collagen. J. Biomater. Appl. 15, 187–229. https://doi.org/10.1106/5JUJ-TFJ3-JVVA-3RJ0.

Zioupos, P., Currey, J.D., 1998. Changes in the stiffness, strength, and toughness of human cortical bone with age. Bone 22, 57–66. https://doi.org/10.1016/S8756-3282(97)00228-7.

Zioupos, P., Currey, J.D., Hamer, A.J., 1999. The role of collagen in the declining mechanical properties of aging human cortical bone. J. Biomed. Mater. Res. 45, 108–116. https://doi.org/10.1002/(sici)1097-4636(199905)45:2<108::aid-jbm5>3.0.co;2-a.